Nanoscale

Microwave synthesized magnetic tubular carbon nanocomposite fabrics toward electrochemical energy storage†

Jiahua Zhu,[a] Minjiao Chen,[a] Narendranath Yerra,[ab] Neel Haldolaarachchige,[c] Sameer Pallavkar,[a] Zhiping Luo,[d] Thomas C. Ho,[a] Jack Hopper,[a] David P. Young,[c] Suying Wei*[b] and Zhanhu Guo*[a]

Contrary to the helical carbon structure from pure cotton fabrics under microwave heating and radical oxidized ignition of nanoparticles from conventional heating, magnetic carbon tubular nanocomposite fabrics decorated with uniformly dispersed Co–Co_3O_4 nanoparticles were successfully synthesized *via* a microwave heating process using cotton fabric and inorganic salt as precursors, which have shown better anti-corrosive performance and demonstrated great potential as novel electrochemical pseudocapacitor electrode.

The ever increasing demand for high-power energy resources in hybrid electric vehicles has triggered great interest in developing supercapacitors with high power supply, long term stability and environmental benign nature. Depending on the electroactivity of electrode materials, supercapacitors could be either electrostatic double layer type (EDLS) without an electrochemical reaction or faradic type (FS) with reactions between electrode and electrolyte.[1] The current FS supercapacitors usually suffer from low power density due to the low electrical conductivity and poor cycling stability because the redox reaction occurs at the electrode.[1a,2] To overcome these challenges, extensive attempts have been made to design novel electrode materials. The major theme is to prepare high capacitance materials by incorporating pseudoactive metal oxides[3] or conductive polymer nanostructures[4] into a conductive carbon matrix. With combined merits of pseudoactive materials (large faradic capacitance) and carbon (high conductivity and large specific surface area), these composite electrodes have demonstrated an enhanced electrochemical capacitance performance. Higher loading of metal oxides is often required to achieve higher energy density. Meanwhile, the charge/discharge rate capability and cycling performance of electrodes are sacrificed because of the large volume changes of oxides occurring during charge–discharge cycles.[5] Therefore, a hybrid structure design with individually embedded metal oxide nanostructures on a flexible conductive substrate is desired. With such a structure, the volume change induced inner stress between metal oxides during charge/discharge could be avoided due to the existence of a buffer spacing between isolated nanostructures provided by the flexible substrate. At the same time, the electron conduction between nanostructure and conductive substrate could be maintained for stable cycling performance.

Besides the integration structure pattern of the pseudoactive component and conductive substrate, the hybrid morphology control is equally important to enhance the capacitance performance. A porous structure is often introduced to enlarge the reactive surface area and prompt electrolyte ion diffusion, which allows more electroactive materials to participate in the reaction and generates larger current density. The template method is a general approach that has been used to synthesize electroactive materials with porous structures, such as hierarchical porous graphitic carbon,[6] arrayed RuO_2 nanotubes,[7] MnO_2 nanosheets,[8] Ni–NiO core–shell particles[9] and Au–CNT hybrid arrays.[10] However, this template approach usually suffers from high cost and complicated operations. Methods to prepare carbon based metal oxide nanocomposites include thermal decomposition,[11] self-assembly,[12] electrochemical deposition,[13] and layer-by-layer technique.[14] All these different methods allow a better control on nanostructures. However, they are either too inefficient for scale-up production or require multiple skilful processes for successful synthesis. Until now, it is still a challenge to produce porous nanocomposites with individually dispersed nanostructures on a flexible and conductive

[a]Integrated Composites Laboratory (ICL), Dan F Smith Department of Chemical Engineering, Lamar University, Beaumont, Texas 77710, USA. E-mail: zhanhu.guo@lamar.edu; Tel: +1-409-880-7654

[b]Department of Chemistry and Biochemistry, Lamar University, Beaumont, Texas 77710, USA. E-mail: suying.wei@lamar.edu; Tel: +1-409-880-7976

[c]Department of Physics and Astronomy, Louisiana State University, Baton Rouge, Louisiana 70803, USA

[d]Department of Chemistry and Physics, Fayetteville State University, Fayetteville, North Carolina, 28301, USA

substrate. Microwave with electromagnetic frequencies ranging from 0.3 to 300 GHz has been a promising technology for manufacturing nanomaterials with its extremely fast heating and cooling rates, which could not be achieved in a conventional heating process with a thermal diffusion controlled heating rate. In the microwave heating process, the average microwave power absorption value or the heating potential depends on the dielectric properties of the material, frequency of the microwave, and the electric field intensity,[15] which is given by eqn (1):

$$Q_{avg} = \omega \varepsilon_0 \varepsilon'' E_{rms}{}^2 \qquad (1)$$

where Q_{avg} is the average microwave power absorption or the heating potential in W m^{-3}, ω is the angular frequency rad s^{-1}, ε_0 is the permittivity of free space (8.85×10^{-12} F m^{-1}), ε'' is the relative dielectric loss factor of the absorbing media, and E_{rms} is the electric field intensity in V m^{-1}. Along a given reaction, the reactants and intermediates can have different dielectric constants. Microwaves could selectively couple with the intermediate in the transition state and overcome the high activation energies for product formation.[16] Besides, the microwave heating reduces the overall thermal gradients in the reaction and thus yield more uniform products.[17] Various unique nanostructures have been synthesized using microwave energy, for example, core–shell Au–Pd bimetallic and Fe–cementite nanoparticles,[18] ZnS and ZnSe nanowires, CdSe nanorods,[19] CoFe$_2$O$_4$ nanoparticles,[20] Co$_3$O$_4$ rods,[21] and tellurium nanorods and nanowires.[22] To the best of our knowledge, this is the first report on the carbon fabric nanocomposite made from microwave heating for electrochemical energy storage.

Here, magnetic carbon microtubular nanocomposites with Co–Co$_3$O$_4$ nanoparticles synthesized by a microwave energy assisted heating method was reported and compared with the conventional heating process. Briefly, commercial T-shirt cotton fabric and cobalt nitrate served as carbon and cobalt precursors, which were converted to carbon fabric nanocomposites with doped metal/metal oxide nanostructures by both the microwave heating process (the products denoted as MTNs) and conventional heating process (the products denoted as MTNs-C). The detailed synthetic procedures are described in the ESI, S1.2.† These composite electrodes, envisioned to combine pseudocapacitance of decorated metal oxide nanoparticles and electrostatic double layer capacitance of carbon matrix, are characterized using different techniques such as cyclic voltammetry, galvanostatic charge/discharge and electric impedance spectroscopy, and their electrochemical energy storage performances are evaluated.

Fig. 1 shows the SEM images of nanocomposites synthesized from microwave heated Co(NO$_3$)$_2$-cotton fabrics. FT-IR spectrum analysis reveals that the organic functional groups of the cotton fabric have been eliminated and converted to carbon, Fig. S1.† The open tube structure could be clearly observed, Fig. 1a. The microtubes exhibit an average diameter of about 10 μm and length of larger than 100 μm. Fig. 1b shows the particle distribution on the microtube. The particles are either uniformly distributed on both sides of the tube surface or
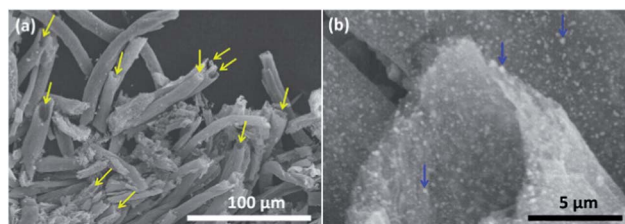
Fig. 1 SEM images of (a) microtube shaped MTNs, (b) magnetic nanoparticles embedded in the carbon microtube wall and partially adhered to the surface.

embedded on the tube wall. This unique open structure endows an efficient charge transfer between the nanoparticles and electrolyte. Meanwhile, the carbon matrix serves as a cushion to reduce the structural damage from the volume change of the nanoparticles during the charge/discharge process.[23] Meanwhile, it is interesting to observe that the cotton fabric (without doping) after microwave annealing are mostly helical rather than tubular in structure, Fig. S2a and b,† indicating that the doping materials have a significant effect on the formation of microtubular structure.

Fig. 2a shows a typical transmission electron microscopy (TEM) image of MTNs. The nanoparticles are individually dispersed in the carbon matrix with an average diameter of 43.5 nm. Using a conventional annealing process in the tube furnace using H$_2$(5%)/Ar purging gas at the heating rate of 10 °C min^{-1} and naturally cooling down, the final products were burned out immediately after exposing to air, indicating that the as-produced nanoparticles were not well protected by a solid carbon shell. Following the same procedure but switching the purging gas to ultra-high purity nitrogen, the final products were observed to be more stable in air. However, the particle
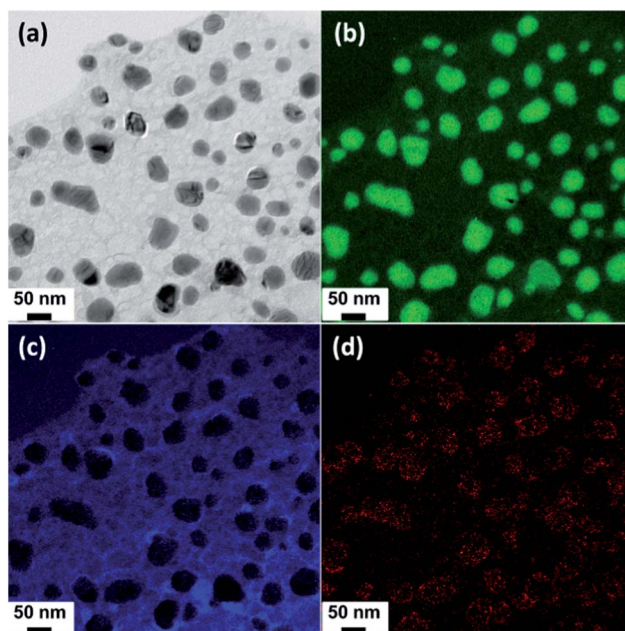
Fig. 2 EFTEM images of the MTNs: (a) zero loss image, (b) Co mapping, (c) C mapping, and (d) O mapping.

size distributes in a much wider range together with serious agglomeration, Fig. S3.† These phenomena further demonstrate that microwave heating reduces overall thermal gradients in the reaction and thus causes more uniform products.[17] Furthermore, both MTNs from microwave heating and MTNs-C from conventional heating were subjected to an anti-corrosion test in 1.0 M HCl. Results reveal that the MTNs exhibit much better stability in acidic solution than that of MTNs-C, Fig. S4.† The pink MTNs-C vial indicates that the cobalt nanoparticles have reacted with HCl, while the MTNs vial still remains colorless indicating that the Co nanoparticles have been well protected by the carbon shell and thus exhibit excellent stability in corrosive media. Attracted by the unique structural and chemical properties of MTNs, energy filter TEM (EFTEM) was conducted to identify the elemental distribution. The strong contrast of Co mapping clearly indicates that the Co element is individually distributed on the carbon substrate, Fig. 2b. Microwave energy initiates a uniform nucleation and fast nanoparticle growth once overcoming the thermodynamic barriers.[16b] Fig. 2c shows a continuous carbon substrate with closed holes of the exact size of nanoparticles, revealing that the nanoparticle growth penetrates into the carbon substrate without breaking the carbon continuity. This is critically important to maintain the flexibility of MTN fabrics. The O mapping, Fig. 2d, matches the shape of the nanoparticles in Fig. 2b, revealing partial oxidization of the Co nanoparticles.

During annealing, the graphitized carbon either grows along the magnetic nanoparticle surface to form a compact core–shell structure or grows out of the surface to form a hollow tube structure. The high-resolution TEM (HRTEM) image, Fig. 3a, reveals the core–shell structure of the magnetic nanoparticles with a saturated magnetization of 62.0 emu g^{-1}, Fig. S5,† where

the magnetic core is covered by a compact graphitized carbon shell with an interplanar spacing of 3.50 Å. The shell thickness is about 6 nm. Focusing on the inside magnetic core, Fig. 3b, the clear lattice fringe of 2.05 Å indicates the (111) crystal plane of Co (PDF#15-0806). In the inset of Fig. 3b, which shows the edge of the magnetic core where graphitic carbon is not fully covered, a lattice fringe of 2.42 Å reveals the (311) crystal plane of cobalt oxide (PDF#42-1467). All these results demonstrate that the magnetic core is a combination of cobalt and cobalt oxide, which has been further confirmed by XRD analysis, Fig. S6.† Fig. 3c shows a unique graphitized carbon nanotube-like structure growing from the catalytic Co nanoparticle surface. The tube growth mechanism follows a base-[24] rather than tip-[25] growth model since the catalyst particles are not observed at the tip or middle of the tube. This unique structure prevents particle agglomeration and thus more of the oxide surface could be exposed and utilized as reaction sites to improve the capacitance performance. Selected area electron diffraction (SAED) pattern of the MTNs, Fig. 3d, only shows the crystalline planes of the Co (111, 200, and 220) (PDF#15-0806) while Co_3O_4 is not clearly observed probably due to the fact that the area taken for SAED is well protected by a compact carbon shell so that oxidation did not occur in that specific area. Further evidence confirming the existence of Co_3O_4 in MTNs comes from the Raman spectra analysis, Fig. S7,† where the characteristic E_g, F_{2g}^1, A_{1g} modes of Co_3O_4 crystalline structure were identified.[26]

To highlight the merits of this hybrid architecture serving as supercapacitor electrode, the electrochemical tests were carried out in a three-electrode configuration with a Pt wire as counter electrode and a standard calomel reference electrode in 1.0 M KOH electrolyte. Fig. 4a shows the cyclic voltammograms (CVs) of MTNs at voltage scan rates of 5–100 mV s^{-1}. The shape of the curves for MTNs indicates that the capacitive characteristic is
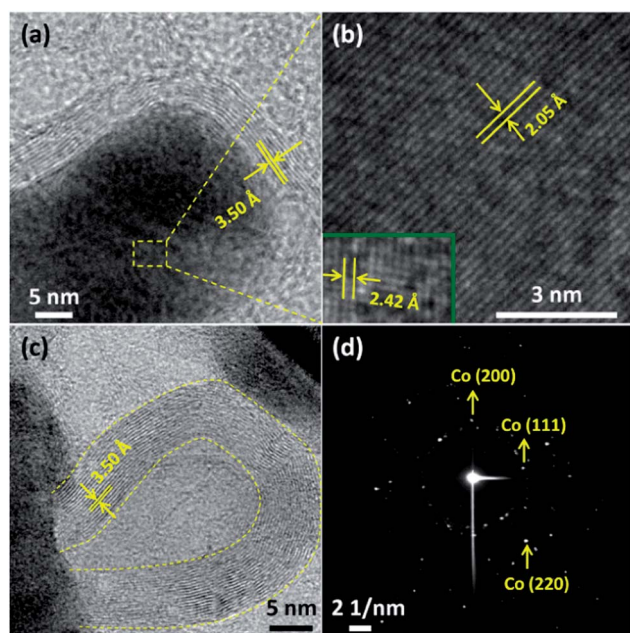
Fig. 3 TEM of (a) the core–shell structure of MTNs, (b) lattice fringe of Co and Co_3O_4, (c) nanotube-like structure grown on particle surface, and (d) selected area electron diffraction (SAED) pattern.
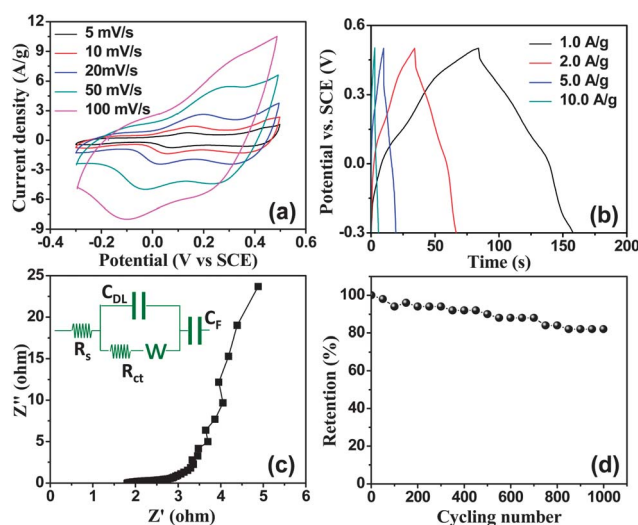
Fig. 4 (a) Cyclic voltammograms, (b) charge/discharge, (c) electrochemical impedance spectroscopy (EIS) and the inset shows the equivalent circuit model for the impedance spectra, and (d) cycling performance of MTNs in 1.0 M KOH electrolyte.

typically a pseudocapacitor, which is different from that of an electric double-layer capacitor with rectangular CV curve.[1,27] It was found that the CV integrated area of MTNs is apparently larger than that of pure carbon electrode at the same scan rate, Fig. S8,† which is due to the redox reaction between the Co_3O_4 nanoparticles and OH^- from the electrolyte. The Co is not involved in the electrochemical reaction. This enlarged CV area leads to a much larger pseudocapacitance of 93.4 F g^{-1} as compared to pure carbon fabric of 2.2 F g^{-1} at a voltage scan rate of 5 mV s^{-1}. The specific capacitance is calculated using eqn (2):

$$C_s = \frac{\int i \, dV}{2 \times m \times \Delta V \times S} \quad (2)$$

where C_s is the specific capacitance in F g^{-1}, $\int i \, dV$ is the integrated area of the CV curve, m is the mass of the electrode material in g (80% of the total mass, refer to electrode preparation in ESI†), ΔV is the scanned potential window in V, and S is the scan rate in V s^{-1}. Two pairs of redox peaks were observed in each scan rate, which correspond to the reversible reactions between different cobalt oxide states according to the following reactions:[28]

$$Co_3O_4 + OH^- + H_2O \leftrightarrow 3CoOOH + e^- \quad (a)$$

$$CoOOH + OH^- \leftrightarrow CoO_2 + H_2O + e^- \quad (b)$$
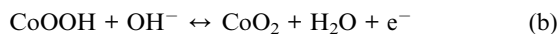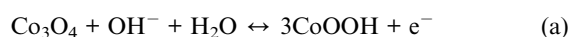
With increasing scan rate, two anodic peaks merge to one peak and cathodic peaks shift toward negative potential. In addition, the peak potential separation ($\Delta E_p = E_{pa} - E_{pc}$; E_{pa} is the anodic peak potential and E_{pc} is the cathodic peak potential) increases with increasing potential scan rate. All these characteristics suggest that the redox process is quasi-reversible rather than a reversible reaction (peak potential will not change in reversible reactions).[29]

Fig. 4b shows the galvanostatic charge–discharge curves of MTNs measured at different current densities from 1.0–10.0 A g^{-1} within the potential range of −0.3 to 0.5 V (vs. SCE) in 1.0 M KOH electrolyte. The discharge curves display a small potential drop at the very beginning of the discharge process, which was caused by the internal resistance of the electrode.[30] The subsequent slower potential decay demonstrates the pseudocapacitive feature of the electrode, which is responsible for longer charge/discharge durations and thus higher energy density.[31] The specific capacitance is calculated from charge/discharge curves according to eqn (3):

$$C_s = \frac{i \times \Delta t}{m \times \Delta V_1} \quad (3)$$

where C_s is the specific capacitance in F g^{-1}, i is the discharge current in A, Δt is the discharge time in s, m is the mass of the electrode material in g and ΔV_1 is potential drop during discharge in V. The C_s and the corresponding energy density (E) and power density (P) calculated from different current densities are summarized in Table 1. E and P are calculated following the method described in previous literature (refer to ESI† for calculation equations).[32] The highest capacitance of 92.5 F g^{-1}

is obtained at the lowest current density of 1 A g^{-1}, which corresponds to a very high energy density of 8.2 W h kg^{-1}. The superior electrochemical performance of MTNs is attributed to the following merits: (1) most of the nanoparticles are exposed on the microtubule surface that allows more metal oxide nanoparticles to participate in the redox reaction; (2) microtube structure of MTNs provides a fast channel for ions being transferred from electrolyte to the inner surface of the electrode; (3) highly conductive graphitized carbon substrate arising from the extremely fast heating and cooling rates of microwave annealing ensures efficient electron transportation during charge/discharge process. The capacitance performance of MTNs is slightly lower compared to some of the reported Co_3O_4 nanocomposites, such as Co_3O_4/graphene[33] and mesoporous Co_3O_4 nanoparticles.[34] Considering the limited amount of surface metal oxides participating in the redox reaction, the interfacial redox reaction is much more efficient than other nanostructures. Besides, the economic raw materials, facile processing technique and satisfactory capacitance performance mean that MTNs are advantageous over others in terms of manufacturing cost and long term stability.

Electrochemical impedance spectroscopy (EIS) was examined in Fig. 4c to better understand the capacitive behavior of MTNs. The impedance spectrum is composed of one semicircle at high frequency and followed by a linear part at low-frequency. The semicircle at high frequency indicates the appreciable contribution of the composite interfacial impedance. An equivalent circuit, inset of Fig. 4c, is proposed to fit the impedance spectra. The equivalent circuit is composed of a solution resistance, R_s, a double layer capacitance, C_{DL}, a finite-length Warburg diffusion element, W, an electrode/electrolyte interfacial charge transfer resistance, R_{ct}, and a faradic capacitance, C_F. The complicated electrochemical process and mass transfer occurring within the microtubule and at the interface were simplified as interfacial impedance consisting of C_{DL} in parallel with a serial combination of W and R_{ct}. The equivalent circuit was then completed by adding this composite interfacial impedance in series with R_s and C_F. The fitting results for each parameter are summarized in Table 1. Both R_s and R_{ct} are very small, indicating a low internal resistance within the system. The relatively larger R_s indicates that the major resistance comes from the electrolyte solution. The smaller R_{ct} reveals low charge transfer resistance at the electrode/electrolyte interface during charge/discharge, which is attributed to the tubular

Table 1 C_s, E and P of MTNs at different current densities

Current density, A g^{-1}	C_s, F g^{-1}	E, W h kg^{-1}	P, W kg^{-1}
1	92.5	8.2	400
2	81.3	7.2	800
5	60.0	5.3	2000
10	35.6	3.2	4000

R_s, Ω	C_{DL}, F	R_{ct}, Ω	W	C_F, F
1.88	0.008	0.62	0.93	0.63

open structure of the electrode material with fully exposed nanoparticles decorating the tube surface. The C_{DL} is negligible as compared to C_F indicating that the faradic capacitance dominates the whole capacitor performance arising from the redox reaction at the interface. Cycling life tests over 1000 cycles at 2.0 A g^{-1} are shown in Fig. 4d. The MTNs exhibit a good long-term stability, as 82% of the capacitance is maintained after 1000 cycles. The high cycling performance may be attributed to the efficient buffering effect of carbon microtube that compromises the volume change of Co_3O_4 during charge and discharge processes as well as the high electrical conductivity of the carbon substrate.[23]

In conclusion, a new flexible carbon microtubule nanocomposite fabric decorated with uniform Co/Co_3O_4 nanoparticles have been synthesized *via* a microwave assisted annealing process. This hybrid fabric could be fabricated into electrodes for wearable energy storage device applications. The microwave assisted annealing process favors better control of particle size and distribution uniformity than the conventional annealing process. More importantly, the nanoparticles are better protected from a microwave process and exhibit excellent anti-corrosion performance in acid. These findings are very encouraging in view of the better nanostructure control, enhanced anti-corrosion and superior electrochemical performance by using microwave energy. The hybrid structural design concept is very general and can be readily applied to other materials by simply choosing different inorganic precursors such as $Fe(NO_3)_3$ and $Ni(NO_3)_2$, Fig. S2c and d,† to build hybrid nano- and micro-structures with high capacitance performance, which will be promising for a large spectrum of energy device applications. The mechanism of the salt in controlling the tubular structures is still not clear and needs further explorations.

Acknowledgements

Notes and references

1 (a) G. Wang, L. Zhang and J. Zhang, *Chem. Soc. Rev.*, 2012, **41**, 797; (b) P. Simon and Y. Gogotsi, *Nat. Mater.*, 2008, **7**, 845.

2 (a) Y. Li, B. Tan and Y. Wu, *Nano Lett.*, 2007, **8**, 265; (b) L. L. Zhang and X. S. Zhao, *Chem. Soc. Rev.*, 2009, **38**, 2520; (c) A. S. Arico, P. Bruce, B. Scrosati, J.-M. Tarascon and W. van Schalkwijk, *Nat. Mater.*, 2005, **4**, 366; (d) N.-S. Choi, Z. Chen, S. A. Freunberger, X. Ji, Y.-K. Sun, K. Amine, G. Yushin, L. F. Nazar, J. Cho and P. G. Bruce, *Angew. Chem., Int. Ed.*, 2012, **51**, 9994.

3 (a) G. Yu, L. Hu, M. Vosgueritchian, H. Wang, X. Xie, J. McDonough, X. Cui, Y. Cui and Z. Bao, *Nano Lett.*, 2011, **11**, 2905; (b) J. Mu, B. Chen, Z. Guo, M. Zhang, Z. Zhang, P. Zhang, C. Shao and Y. Liu, *Nanoscale*, 2011, **3**, 5034; (c) A. Reddy, M. Shaijumon, S. Gowda and P. Ajayan, *Nano Lett.*, 2009, **9**, 1002; (d) X. Zhao, B. M. Sanchez, P. Dobson and P. Grant, *Nanoscale*, 2011, **3**, 839; (e) H. Huang and X. Wang, *Nanoscale*, 2011, **3**, 3185; (f) Y. Wang, H. Zhang, L. Lu, L. Stubbs, C. Wong and J. Lin, *ACS Nano*, 2010, **4**, 4753; (g) J. Bae, M. Song, Y. Park, J. Kim, M. Liu and Z. Wang, *Angew. Chem., Int. Ed.*, 2011, **50**, 1683; (h) H. Qi, X. Roy, K. Shopsowitz, J. Hui and M. MacLachlan, *Angew. Chem., Int. Ed.*, 2010, **49**, 9740; (i) F. Xia, X. Hu, Y. Sun, W. Luo and Y. Huang, *Nanoscale*, 2012, **4**, 4707; (j) D. Deng and J. Lee, *Angew. Chem., Int. Ed.*, 2009, **48**, 1660; (k) Q. Lu, M. Lattanzi, Y. Chen, X. Kou, W. Li, X. Fan, K. Unruh, J. Chen and J. Xiao, *Angew. Chem., Int. Ed.*, 2011, **50**, 6847; (l) J. Zhu, M. Chen, H. Qu, Z. Luo, S. Wu, H. A. Colorado, S. Wei and Z. Guo, *Energy Environ. Sci.*, 2013, **6**, 194.

4 (a) K. Xie, J. Li, Y. Lai, Z. Zhang, Y. Liu, G. Zhang and H. Huang, *Nanoscale*, 2011, **3**, 2202; (b) Y. Li, Y. Fang, H. Liu, X. Wu and Y. Lu, *Nanoscale*, 2012, **4**, 2867; (c) Y. Wang, H. Li and Y. Xia, *Adv. Mater.*, 2006, **18**, 2619; (d) Q. Wu, Y. Xu, Z. Yao, A. Liu and G. Shi, *ACS Nano*, 2010, **4**, 1963; (e) L. Fan, Y. Hu, J. Maier, P. Adelhelm, B. Smarsly and M. Antonietti, *Adv. Funct. Mater.*, 2007, **17**, 3083; (f) D. Wang, F. Li, J. Zhao, W. Ren, Z. Chen, J. Tan, Z. Wu, I. Gentle, G. Lu and H. Cheng, *ACS Nano*, 2009, **3**, 1745; (g) M. Hughes, G. Chen, M. Shaffer, D. Fray and A. Windle, *Chem. Mater.*, 2002, **14**, 1610; (h) J. Zhu, M. Chen, H. Qu, X. Zhang, H. Wei, Z. Luo, H. Colorado, S. Wei and Z. Guo, *Polymer*, 2012, **53**, 5953; (i) H. Wei, X. Yan, S. Wu, Z. Luo, S. Wei and Z. Guo, *J. Phys. Chem. C*, 2012, **116**, 25052.

5 A. E. Fischer, K. A. Pettigrew, D. R. Rolison, R. M. Stroud and J. W. Long, *Nano Lett.*, 2007, **7**, 281.

6 D. W. Wang, F. Li, M. Liu, G. Q. Lu and H.-M. Cheng, *Angew. Chem.*, 2008, **120**, 379.

7 C.-C. Hu, K.-H. Chang, M.-C. Lin and Y.-T. Wu, *Nano Lett.*, 2006, **6**, 2690.

8 G. Zhao, J. Li, L. Jiang, H. Dong, X. Wang and W. Hu, *Chem. Sci.*, 2012, **3**, 433.

9 J.-H. Kim, S. H. Kang, K. Zhu, J. Y. Kim, N. R. Neale and A. J. Frank, *Chem. Commun.*, 2011, **47**, 5214.

10 M. M. Shaijumon, F. S. Ou, L. Ci and P. M. Ajayan, *Chem. Commun.*, 2008, 2373.

11 (a) J. Zhu, S. Wei, H. Gu, S. B. Rapole, Q. Wang, Z. Luo, N. Haldolaarachchige, D. P. Young and Z. Guo, *Environ. Sci. Technol.*, 2012, **46**, 977; (b) J. Zhu, H. Gu, S. B. Rapole, Z. Luo, S. Pallavkar, N. Haldolaarachchige, T. J. Benson, T. C. Ho, J. Hopper, D. P. Young, S. Wei and Z. Guo, *RSC Adv.*, 2012, **2**, 4844.

12 (a) J. Li, S. Tang, L. Lu and H. C. Zeng, *J. Am. Chem. Soc.*, 2007, **129**, 9401; (b) D. Wang, R. Kou, D. Choi, Z. Yang, Z. Nie, J. Li, L. V. Saraf, D. Hu, J. Zhang, G. L. Graff, J. Liu, M. A. Pope and I. A. Aksay, *ACS Nano*, 2010, **4**, 1587.

13 (a) E. S. Steigerwalt, G. A. Deluga and C. M. Lukehart, *J. Phys. Chem. B*, 2002, **106**, 760; (b) J. Yan, H. Zhou, P. Yu, L. Su and L. Mao, *Electrochem. Commun.*, 2008, **10**, 761.

14 N. Du, H. Zhang, B. D. Chen, X. Y. Ma, Z. H. Liu, J. B. Wu and D. R. Yang, *Adv. Mater.*, 2007, **19**, 1641.

15 (a) I. Plazl, G. Pipus and T. Koloini, *AIChE J.*, 1997, **43**, 754; (b) A. C. Metaxas and R. J. Meredith, *Power Engineering Series 4*, London, UK, 1983; (c) Z. Hashisho, M. Rood and L. Botich, *Environ. Sci. Technol.*, 2005, **39**, 6851; (d) M. D. Turner, R. L. Laurence, W. C. Conner and K. S. Yngvesson, *AIChE J.*, 2000, **46**, 758; (e) T. Ohgushi, Y. Sakai, Y. Adachi and H. Satoh, *J. Phys. Chem. C*, 2009, **113**, 8206.

16 (a) A. Loupy, *Microwaves in Organic Synthesis*, Wiley-VCH, Weinheim, Germany and Cambridge, U.K., 2002; (b) J. Gerbec, D. Magana, A. Washington and G. Strouse, *J. Am. Chem. Soc.*, 2005, **127**, 15791.

17 (a) W. Chen, J. Lee and Z. Liu, *Chem. Commun.*, 2002, 2588; (b) B. Hu, S. Wang, K. Wang, M. Zhang and S. Yu, *J. Phys. Chem. C*, 2008, **112**, 11169; (c) P. Raveendran, J. Fu and S. Wallen, *Green Chem.*, 2006, **8**, 34.

18 (a) R. Harpeness and A. Gedanken, *Langmuir*, 2004, **20**, 3431; (b) J. Zhu, S. Pallavkar, M. Chen, N. Yerra, Z. Luo, H. Colorado, H. Lin, N. Haldolaarachchige, A. Khasanov, T. Ho, D. Young, S. Wei and Z. Guo, *Chem. Commun.*, 2013, **49**, 258.

19 A. B. Panda, G. Glaspell and M. S. El-Shall, *J. Am. Chem. Soc.*, 2006, **128**, 2790.

20 F. Bensebaa, F. Zavaliche, P. L'Ecuyer, R. W. Cochrane and T. Veres, *J. Colloid Interface Sci.*, 2004, **277**, 104.

21 W.-W. Wang and Y.-J. Zhu, *Mater. Res. Bull.*, 2005, **40**, 1929.

22 Y.-J. Zhu, W.-W. Wang, R.-J. Qi and X.-L. Hu, *Angew. Chem.*, 2004, **116**, 1434.

23 (a) H. Kim, D.-H. Seo, S.-W. Kim, J. Kim and K. Kang, *Carbon*, 2011, **49**, 326; (b) W.-L. Yao, J.-L. Wang, J. Yang and G.-D. Du, *J. Power Sources*, 2008, **176**, 369.

24 L. J. Ci, Z. G. Zhao and J. B. Bai, *Carbon*, 2005, **43**, 883.

25 S. Iijima, P. M. Ajayan and T. Ichihashi, *Phys. Rev. Lett.*, 1992, **69**, 3100.

26 (a) T. Yu, Y. W. Zhu, X. J. Xu, Z. X. Shen, P. Chen, C. T. Lim, J. T. L. Thong and C. H. Sow, *Adv. Mater.*, 2005, **17**, 1595; (b) V. G. Hadjiev, M. N. Iliev and I. V. Vergilov, *J. Phys. C: Solid State Phys.*, 1988, **21**, L199.

27 M. M. Noked, S. Okashy, T. Zimrin and D. Aurbach, *Angew. Chem., Int. Ed.*, 2012, **51**, 1568.

28 (a) L. Cao, F. Xu, Y. Y. Liang and H. L. Li, *Adv. Mater.*, 2004, **16**, 1853; (b) C. Lin, J. A. Ritter and B. N. Popov, *J. Electrochem. Soc.*, 1998, **145**, 4097.

29 Y. Gao, S. Chen, D. Cao, G. Wang and J. Yin, *J. Power Sources*, 2010, **195**, 1757.

30 L. Zhang and G. Shi, *J. Phys. Chem. C*, 2011, **115**, 17206.

31 S. Chen, J. Zhu and X. Wang, *J. Phys. Chem. C*, 2010, **114**, 11829.

32 J. Zang and X. Li, *J. Mater. Chem.*, 2011, **21**, 10965.

33 J. Yan, T. Wei, W. Qiao, B. Shao, Q. Zhao, L. Zhang and Z. Fan, *Electrochim. Acta*, 2010, **55**, 6973.

34 M.-b. Zheng, J. Cao, S.-t. Liao, J.-s. Liu, H.-q. Chen, Y. Zhao, W.-j. Dai, G.-b. Ji, J.-m. Cao and J. Tao, *J. Phys. Chem. C*, 2009, **113**, 3887.